Application of a Monotonic Upstream-biased Transport Scheme to Three-Dimensional Constituent Transport Calculations

DALE J. ALLEN*

Applied Research Corporation, Landover, Maryland

ANNE R. DOUGLASS, RICHARD B. ROOD AND PAUL D. GUTHRIE

NASA/Goddard Space Flight Center, Greenbelt, Maryland

(Manuscript received 19 September 1990, in final form 15 March 1991)

ABSTRACT

The application of van Leer's scheme, a monotonic, upstream-biased differencing scheme, to three-dimensional constituent transport calculations is shown. The major disadvantage of the scheme is shown to be a self-limiting diffusion. A major advantage of the scheme is shown to be its ability to maintain constituent correlations. The scheme is adapted for a spherical coordinate system with a hybrid sigma-pressure coordinate in the vertical. Special consideration is given to cross-polar flow. The vertical wind calculation is shown to be extremely sensitive to the method of calculating the divergence. This sensitivity implies that a vertical wind formulation consistent with the transport scheme is essential for accurate transport calculations. The computational savings of the time-splitting method used to solve this equation are shown. Finally, the capabilities of this scheme are illustrated by an ozone transport and chemistry model simulation.

1. Introduction

Constituent transport and chemistry model experiments help explain the processes affecting the distribution of ozone and other chemical constituents. An analysis of the results of these experiments is essential to interpret satellite observations, to calculate constituent budgets, and to separate the effects of chemistry and transport. The solution of the constituent continuity equation is an integral part of these calculations. At NASA/Goddard Space Flight Center (GSFC), three-dimensional constituent evolution is being modeled by solving the constituent continuity equation with transport winds from an assimilated data model (Rood et al. 1989a,b). The successes and failures in modeling ozone, hydrochloric acid, chlorine-containing species, and other species during the 1978/79 and 1988/89 winters are documented by Rood et al. (1989a,b; 1990) and Kaye et al. (1989a,b; 1990). These results were obtained with a spectral transport scheme.

Spectral transport generates negative constituent densities. Although these values were eliminated by using Forester's filter (Forester 1977) and filling, the use of filters that are a function of constituent distribution corrupts the correlations between constituents. Correlations are a powerful interpretive aid, and their maintenance is demanded by physical and chemical theory (Fahey 1990a,b).

Furthermore, the assimilated data used to provide the advecting winds contain small-scale noise, especially near the poles. A spectral fit to noisy data propagates the noise globally. Transport with these spectral winds leads to spurious constituent density fluctuations near the poles. Therefore, a scheme that uses a gridpoint approach is expected to improve the behavior of the calculations near the pole.

Because of these problems a switch was made to van Leer's scheme (van Leer 1974; 1977a,b; 1979), an upstream-biased monotonic gridpoint transport scheme. This scheme is representative of a class of upstream monotonic methods. A monotonic scheme does not generate new maxima or minima and therefore does not require a filling algorithm. The upstream-bias provides a "Lagrangian character" and reduces phase errors to near zero (Rood 1987; Thompson 1984), but it does introduce diffusive errors. The gridpoint scheme handles the noise better because of its local nature. A description of the scheme, its diffusive properties, and its extension to spherical coordinates follows. The extreme sensitivity of the vertical transport calculation and the method of time splitting (i.e., the breaking of the three-dimensional advection operator into three one-dimensional operators) are discussed. Finally,

* This research was done under contract at the Goddard Space Flight Center, Greenbelt, Maryland.

Corresponding author address: Dr. Richard B. Rood, NASA/Goddard Space Flight Center, Code 916, Greenbelt, MD 20771.

preliminary results from this transport method are highlighted by comparing model calculations with observations.

2. van Leer's scheme

The transport scheme was developed by Bram van Leer (van Leer 1974; 1977a,b; 1979). Details of the derivation that follow are taken from a paper by Hawley et al. (1984). The one-dimensional equation,

$$\frac{\partial C}{\partial t} + \frac{\partial}{\partial x}(uC) = 0, \tag{2.1}$$

may be written as

$$C_{j+1/2}^{n+1} = C_{j+1/2}^{n} - \frac{\Delta t}{\Delta x_{j+1/2}}[(\text{flux})_{j+1} - (\text{flux})_j], \tag{2.2}$$

where $C_{j+1/2}$ equals mass density in box center, $(\text{flux})_j$ equals time-averaged flux across jth boundary, Δt equals time interval between time steps, n equals time step, $\Delta x_{j+1/2}$ equals grid spacing, and u equals transport velocity. The densities are defined at NLON box centers and the velocities and fluxes at NLON + 1 box edges as shown in Fig. 1.

The final expressions for the time-averaged density flux are:

$$(\text{flux})_j = u_j\left[C_{j-1/2}^{n} + \frac{1}{2}\left(1 - \frac{u_j\Delta t}{\Delta x_{j-1/2}}\right)\Delta_{j-1/2}C\right] \qquad u_j > 0. \tag{2.3a}$$

$$(\text{flux})_j = u_j\left[C_{j+1/2}^{n} - \frac{1}{2}\left(1 + \frac{u_j\Delta t}{\Delta x_{j+1/2}}\right)\Delta_{j+1/2}C\right] \qquad u_j < 0, \tag{2.3b}$$

where Δ is an operator that acts on C.

Equations (2.2)–(2.3) represent the movement of mass from one box to another by determining explicitly what percentage of the mass from each box should be moved to the downstream box. The percentage is calculated by estimating the mass density at the box edge at both times n and $n + 1$ and multiplying the average of this value by the wind velocity. The mass density at the box edge is determined with a Taylor's series expansion in time and space about the mass density in the box center at time n. In other words, the slope of the density field $\Delta C/\Delta x$ is extrapolated in the upstream direction to determine the density at the box edge. This Lagrangian calculation is a characteristic of upstream-biased schemes and makes the method ideal for mass conservation even in curvilinear coordinates. However, the upstream calculation is also a source of numerical diffusion. This procedure may be modified to apply to the mixing ratio as will be shown in the section on the solution of Eq. (2.5).

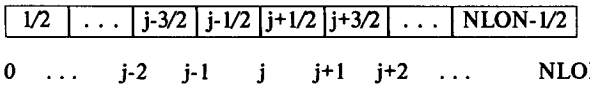

FIG. 1. Diagram defining transport grid.

The slope estimation is crucial to counteract the numerical diffusion. If ΔC is set to zero, the method reduces to simple diffusive upstream differencing (Rood 1987). Several schemes with different expressions for ΔC are described by van Leer (1977b, 1979). The simplest expression that minimizes diffusion and guarantees monotonicity is

$$\Delta_{j-1/2}C = \frac{2(C_{j-1/2} - C_{j-3/2})(C_{j+1/2} - C_{j-1/2})}{C_{j+1/2} - C_{j-3/2}}$$
$$\text{for} \quad (C_{j-1/2} - C_{j-3/2})(C_{j+1/2} - C_{j-1/2}) > 0,$$
$$\text{otherwise} \quad \Delta_{j-1/2}C = 0. \tag{2.4}$$

The conditional test flags regions of buckling. In these regions the extrapolated value of C at the box boundary may not be between the actual values surrounding it. Monotonicity is ensured by setting ΔC to zero in these regions.

The resultant algorithm is less diffusive than simple upstream differencing, but does contain a scale-dependent, self-limiting diffusion. This is illustrated in Fig. 2, which shows the application of the scheme to the one-dimensional advection of a triangular distribution by a constant velocity with cyclic boundary conditions. The base of the triangle is defined with $10X$ grid boxes. The domain is $40X$ grid boxes; $X = 1$ for the standard resolution. The cases $2X$ and $5X$ are two and five times this resolution. Figure 2a shows the field after 10 revolutions at 3 different spatial resolutions. The effect of doubling the resolution quite dramatically improves the retention of the peak.

As stated above, the diffusion is self-limiting. That is, once the transport scheme diffuses a particular distribution to a preferred shape, the magnitude of the diffusion decreases, and the subsequent advection of this shape is essentially perfect. This is explicitly shown in Fig. 2b. This figure shows the $2X$ results from Fig. 2a after 1, 5, 7, and 8 revolutions through the cyclic domain. By the time the triangle has been through 8 revolutions, the clipping of the peak has virtually ceased. A similar calculation with other transport algorithms is discussed in Rood (1987).

Figure 2 demonstrates the basic features of many of the upstream-biased monotonic schemes. A certain number of grid points are needed to resolve the distribution and its slope. Once the distribution has been distorted to the point that the scheme can resolve it, the performance is outstanding. There are essentially no phase errors. Because of this self-limiting diffusion, small-scale structures that are resolved, albeit poorly, in a standard finite-difference calculation are not re-

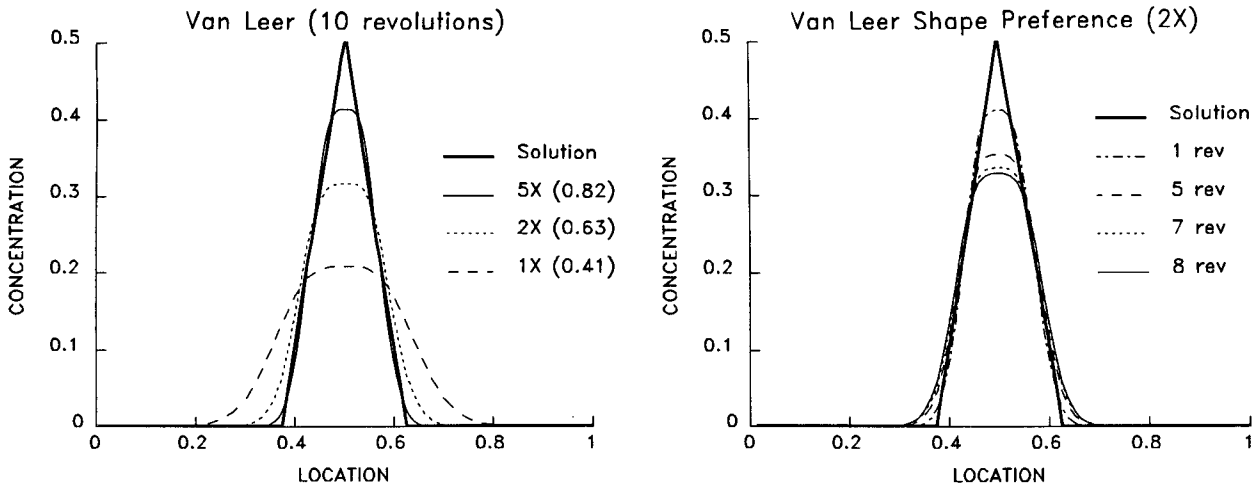

FIG. 2. (a) Triangular distribution initially defined with a $10X$ gridbox base after 10 revolutions at 3 different spatial resolutions through a $40X$ gridbox domain. (b) Same distribution after 1, 5, 7, and 8 revolutions at $2X$ resolution.

solved in an upstream-biased monotonic calculation. Practically, it requires on the order of 3–4 grid points to resolve a peak. Therefore, if it was necessary to resolve atmospheric phenomena on a 4° latitude × 5° longitude scale; then the transport scheme would need to operate with at least twice that resolution.

The extension of van Leer's scheme to curvilinear coordinates will be shown by adapting it to the spherical coordinate system of the assimilated data model (Baker et al. 1987) that produces the input transport winds and temperature fields. This model has eight sigma levels in the troposphere and eleven pressure levels in the stratosphere. The interface pressure is 120 mb and the pressure at the top of the model is 0.305 mb. The three-dimensional constituent continuity equation for mixing ratio in this coordinate system is

$$\frac{\partial D}{\partial t} = -\frac{1}{\Pi}\Bigg[\underbrace{D\frac{\partial \Pi}{\partial t}}_{\text{term 1}} + \underbrace{\frac{\partial}{\partial x}(\Pi u D)}_{\text{term 2}} + \underbrace{\frac{1}{\cos\phi}\frac{\partial}{\partial y}(\Pi \cos\phi v D)}_{\text{term 3}} + \underbrace{\Pi\frac{\partial}{\partial \sigma}(\dot{\sigma} D)}_{\text{term 4}} - \Pi s\Bigg], \quad (2.5)$$

where D equals constituent mixing ratio, u and v are horizontal components of the transport wind, $\dot{\sigma}$ equals vertical component of transport wind, σ equals $(p_k - p_{\text{int}})/\Pi$, Π equals $p_{\text{int}} - p_{\text{top}}$ in the stratosphere and $p_{\text{sfc}} - p_{\text{int}}$ in the troposphere, p_k equals pressure at level k, p_{int} equals pressure at interface between stratosphere and troposphere, p_{sfc} equals surface pressure, p_{top} equals pressure at top of model, and s equals chemical sources and sinks.

This equation is derived from Eq. (2.1) by substituting $M_b D$ for C. Background mass M_b is defined as $100\Delta x\Delta y\Delta p/g$ where g equals gravity, Δx equals the east–west distance across a grid box and is proportional to cosine of latitude, Δy equals the north–south distance across a grid box and is constant, and Δp equals the change in pressure across a grid box. In this coordinate system, $\Delta p = \Pi\Delta\sigma$.

This equation is more complex than Eq. (2.1) because of the vertical coordinate and because the mixing ratio is forecast. Mixing ratio is forecast because it is used in the chemical calculations. A short discussion of the method used to calculate the dynamical terms on the right hand side of Eq. (2.5) follows.

a. Term 1: Surface pressure change

This term is the mixing ratio change due to the temporal change in background mass. It equals zero in the stratosphere and equals $\partial p_{\text{sfc}}/\partial t$ in the troposphere. The calculation of the surface pressure change term [see Eq. (2.9) below], which reduces to the column-averaged divergence, is given in the discussion of term 4.

Terms 2–4 are proportional to the divergence of the constituent flux. They are calculated separately. The general method of calculating these terms independently during transport and chemistry calculations is known as time or operator splitting and is discussed in McRae (1982). This independent calculation of these terms makes it possible to choose a different time step in each direction. Some accuracy is lost when the velocity vector has substantial components in more than one coordinate direction, but the accuracy loss is minor and features are not sheared or disturbed.

b. Term 2: Zonal component of the divergence

The mixing ratio "flux" $(u_j D_j)$ is calculated with Eqs. (2.3)–(2.4) by replacing C_j with D_j. The value for Π is constant in the stratosphere and at the box edges in the troposphere Π is determined by linear interpolation. Each latitude is calculated separately. The

time step at each latitude should be large enough to lessen computational costs but small enough to avoid violating the Courant–Friedrichs–Levy (CFL) stability condition (Haltiner and Williams 1980). Specifically, Δt is reduced by a factor of 5 poleward of 70°. The zonal divergence calculation poleward of 70° requires 55% of the total zonal divergence calculation time on the CRAY Y-MP.

c. *Term 3: Meridional component of the divergence*

The mixing ratio "flux" (v_jD_j) is calculated with Eqs. (2.3)–(2.4) by replacing C_j with D_j, Δx_j with Δy, and u_j with v_j. The value for Π at the box edges in the troposphere is determined by linear interpolation. Cross-polar flow requires special consideration: ΔD is assumed to be zero for the polar box. The polar cap is assumed to be well mixed, and no zonal transport is performed in it. The mixing ratio increase (decrease) in the polar caps due to meridional transport is calculated by summing the mass flow into (out of) the polar cap from the zonal grid points just equatorward of the pole (see Fig. 3). This value is divided by the background mass of the polar cap to determine the mixing ratio change. The background mass in the polar cap is defined to be $100\pi r^2\Delta p/g$ where r is the radius of the polar cap. The mixing ratio change in the polar caps is given by Eq. (2.6) below:

$$D_0^{n+1} - D_0^n = \frac{\pm 2\Delta t}{\alpha[\sin(\Delta\phi)]\text{NLON}} \sum_{i=1}^{\text{NLON}} (\text{mixing ratio flux})_i, \tag{2.6}$$

where the positive (negative) sign is for the north (south) polar cap, $(\text{mixing ratio flux})_i$ equals time-averaged mixing ratio flux across polar cap edge as defined with Eq. (2.3) with C_j replaced by D_j, α equals radius of the earth, NLON equals number of zonal grid points, $\Delta\phi$ equals distance from polar cap edge to pole in radians, and D_0 equals mixing ratio in polar cap.

The distortion introduced by the self-limiting diffusion and the well-mixed approximation are illustrated in Figs. 4a–d, which show a cosine hill being advected over the pole with a nondivergent wind velocity. The initial condition (Fig. 4a), and the hill after 8 (Fig. 4b), 16 (Fig. 4c), and 24 (Fig. 4d) h of integration are shown with a Lambert equal-area projection that is always centered over the center of the cosine hill. The polar cap has a radius of $3\pi\alpha/180$. A similar calculation with a different transport scheme and the same winds was performed by Williamson and Rasch (1989). The distortion due to self-limiting diffusion is minor (compare Figs. 4a and 4b). The hill becomes tearlike and slightly more diffuse as it crosses the pole (Figs. 4c and 4d) due to the well-mixed approximation. Cross-polar flow is calculated accurately enough for our purposes. More accurate results could be obtained by calculating ΔD in the polar box or by choosing a smaller polar cap.

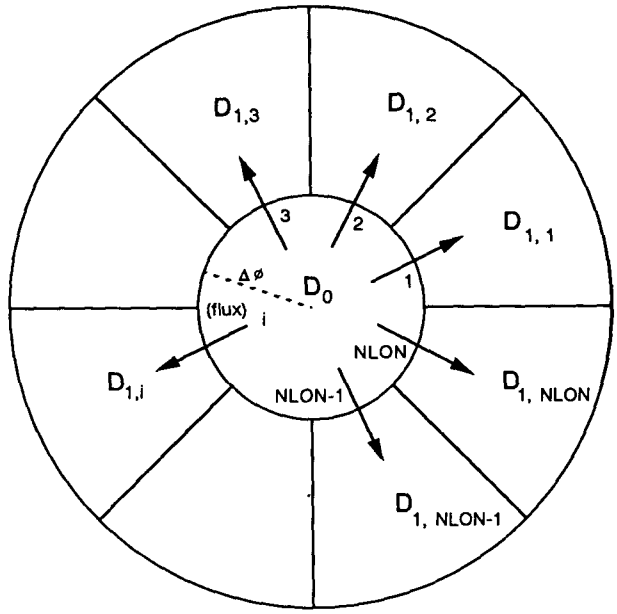

FIG. 3. Diagram defining terms of Eq. (2.6). Equation (2.6) is used to calculate the flow across the South Pole.

d. *Term 4: Vertical component of the divergence*

The vertical transport calculations require $\dot\sigma$ at the interfaces ($k + 1/2$) between the 19 levels (k). The constituent continuity equation (2.5) reduces to the continuity equation (2.7), when it is solved for a constant mixing ratio field with no sources or sinks, (i.e., $\partial D/\partial t = 0$):

$$\frac{\partial \Pi}{\partial t} = -\left[\frac{\partial}{\partial x}(\Pi u) + \frac{1}{\cos\phi}\frac{\partial}{\partial y}(\Pi \cos\phi v) + \Pi\frac{\partial}{\partial\sigma}(\dot\sigma)\right]. \tag{2.7}$$

An expression for the vertical velocity $\dot\sigma$ at any interface ($k + 1/2$) can be obtained by integrating the continuity equation from the top of the model where σ equals -1 and $\dot\sigma$ equals 0 to interface $k + 1/2$; $\partial\Pi/\partial t$ in the troposphere is found by evaluating Eq. (2.8),

$$\Pi\dot\sigma = \int_{-1}^{\sigma}\left[\frac{\partial}{\partial x}(\Pi u) + \frac{1}{\cos\phi}\frac{\partial}{\partial y}(\Pi\cos\phi v)\right] - \begin{cases} 0, \text{ stratosphere} \\ \sigma\dfrac{\partial\Pi}{\partial t}, \text{ troposphere,} \end{cases} \tag{2.8}$$

at the surface where σ equals 1 and $\dot\sigma$ equals zero.

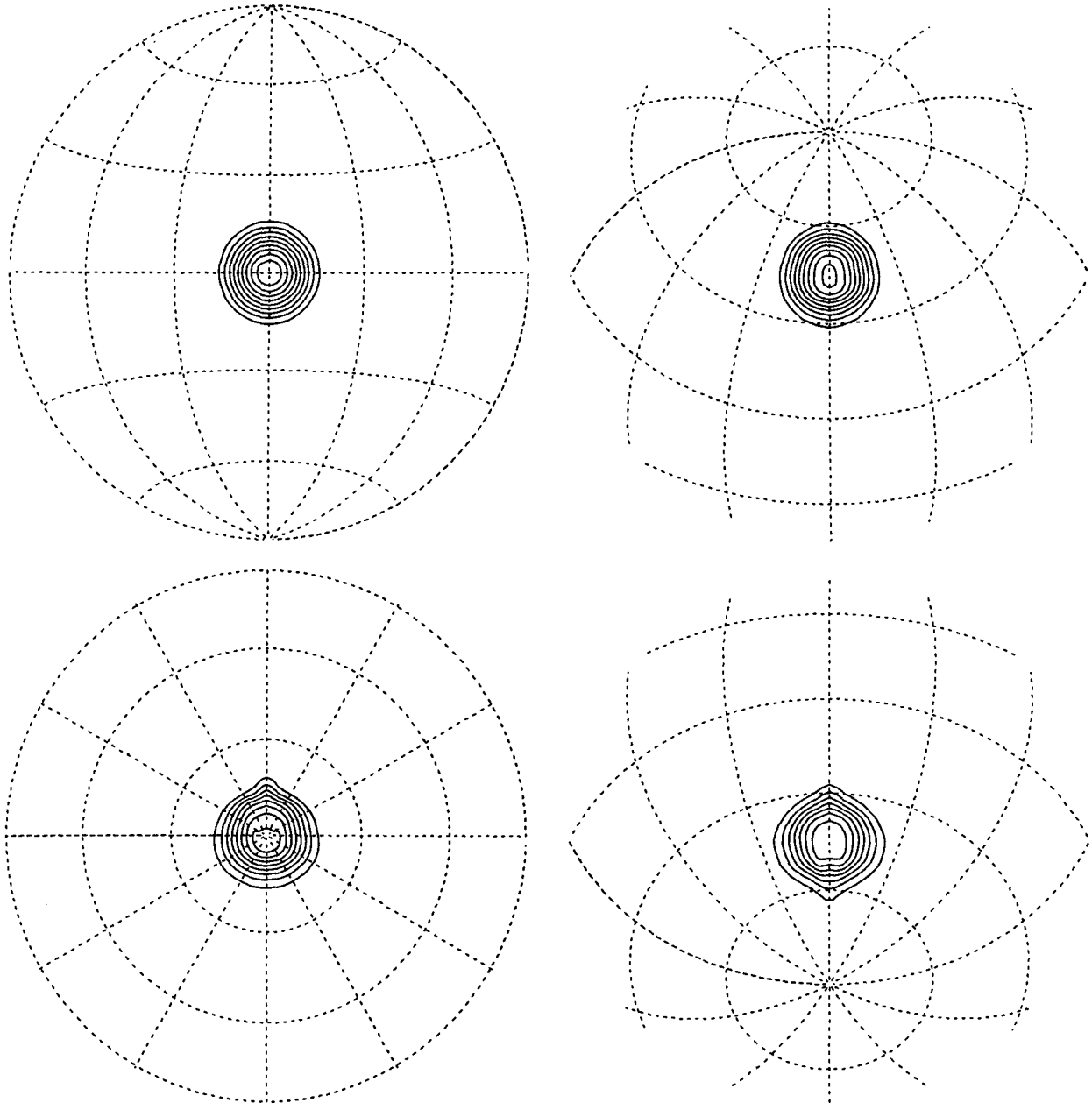

FIG. 4. Lambert equal-area projections of a cosine hill as it is advected over the pole with a nondivergent wind velocity defined with Eqs. (4.2)–(4.3) of Williamson and Rasch (1989). (a) Initial condition as defined by Eqs. (4.4)–(4.5) of Williamson and Rasch (1989). (b) Cosine hill after 8 h. (c) Cosine hill after 16 h. (d) Cosine hill after 24 h.

This column-averaged divergence, term (2.9),

$$\frac{\partial \Pi}{\partial t} = \frac{\partial p_{\text{sfc}}}{\partial t} = -\int_{-1}^{1} \nabla_\sigma \cdot (\Pi \mathbf{v}) d\sigma, \qquad (2.9)$$

is calculated with two integrals since the definition of Π and σ change across the stratosphere–troposphere interface. The horizontal components of the wind at the interface are obtained via interpolation. The divergence is calculated with van Leer's scheme. The tropospheric integral is calculated with Simpson's rule, while the stratospheric integral is calculated with the modified trapezoidal rule.

In order to conserve mass, the method used to solve the continuity equation (2.8) for the vertical velocity must be consistent with the method used to solve the constituent continuity equation (2.5). In effect, the vertical velocity at each interface is the residual needed to satisfy Eq. (2.7) exactly given our method of horizontal and vertical transport. Alternatively, $\dot{\sigma}$ was cal-

culated to assure that $\partial D/\partial t = 0$ for a field where D is initially constant.

The resulting expression for $\dot{\sigma}$ is

$$\dot{\sigma}_{k-1/2} = \dot{\sigma}_{k+1/2} + \frac{\Delta\sigma_k}{\Pi}\left[\frac{\partial \Pi}{\partial t} + \frac{\partial}{\partial x}(\Pi u_k) + \frac{1}{\cos\phi}\frac{\partial}{\partial y}(\Pi \cos\phi v_k)\right]. \quad (3.0)$$

The integral on the right-hand side of Eq. (2.8) has been broken into separate integrals for each level. The vertical velocity calculation begins at the top interface where $\dot{\sigma} = 0$ and proceeds interface by interface assuring that $\partial D/\partial t = 0$ for each grid box on each level. Finite-difference errors require the vertical velocity at the surface ($\dot{\sigma}_{1/2}$) to be nonzero in order to keep $\partial D/\partial t = 0$ in the lowest level. Operationally, this is not a problem. The horizontal components of the divergence are calculated with van Leer's method. This is consistent with the calculation of the horizontal components of the divergence of the constituent flux discussed earlier.

The mixing ratio "flux" ($\dot{\sigma}_j D_j$) is calculated with Eqs. (2.3)–(2.4) by replacing C_j with D_j, Δx_j with $\Delta\sigma_j$, and u_j with $\dot{\sigma}_j$. Since background density decreases exponentially with height, the conditional test, Eq. (2.4), required to keep mixing ratio monotonic with height is more strict than the test required to keep constituent density monotonic with height. The stricter test ensures that the extrapolated mixing ratio at a box edge is between the actual values surrounding it.

Since the horizontal and vertical transport numerics of the assimilated data and transport model differ, conservation of mass requires the vertical velocities to differ. The vertical velocity fields of the assimilated data and transport models at 40.5 mb on 31 December 1988 are compared in Figs. 5a–c. The fields at this interface and others (not shown) are virtually identical, except near the poles where differences of up to 30% in the magnitude of cell centers indicate that the polar divergence calculation is very sensitive to the algorithm used.

3. Discussion

The impact of van Leer's scheme on our transport calculations was investigated by solving the constituent continuity equation for ozone with a rhomboidal 30 (R30) spectral model, a 4° latitude × 5° longitude van Leer model, and a 2° latitude × 2.5° longitude van Leer model. The calculations were initialized on 28 December 1988. The 2° × 2.5° van Leer calculation was initialized with the method of Douglass et al. (1990). The R30 spectral resolution was used for many of our transport calculations during 1978/79 and 1988/89 winters (Rood et al. 1989a). The R30 spectral calculation required 700 s per day on the ETA-10P. The 2° × 2.5° van Leer calculation required 200 s per day on the ETA-10P.

Figures 6a–d are polar orthographic projections comparing the Northern Hemisphere total ozone columns on 31 January 1989 of the 2° × 2.5° van Leer calculation (Fig. 6a), the 4° × 5° van Leer calculation (Fig. 6b), and the spectral calculation (Fig. 6c), with the Total Ozone Mapping Spectrometer (TOMS) measurements (Fig. 6d). The orthographic projection is chosen to emphasize polar regions.

The distinguishing features in the TOMS measurements are two regions of high total ozone near 60°N, 270°E and 50°N, 150°E, a small region of very low total ozone near 60°N, 10°E, and a meandering region of tight gradients (120°–300°E) that separates the areas of high total ozone from the midlatitudes. Transient depressions of total ozone such as the one near 60°N, 10°E, are called *miniholes* (Newman et al. 1988). Measurements are not available at high latitudes due to polar night.

The 2° × 2.5° van Leer calculation reproduces the location, magnitude, and shape of the minihole and the magnitude and shape of the highs. The highs are slightly displaced to the south. A portion of the polar vortex, which is barely visible in the TOMS measurements, also shows up as the area of low total ozone that extends from 50°N to the pole between 330° and 120°E. The total ozone values in this region are highly correlated with 30-mb potential vorticity. The main features are more diffuse in the calculation than in the measurements. For example, the 120°–300°E total ozone gradient is less distinct, and the highlighted 480 Dobson unit calculation contour encompasses more area than the same measurement contour.

Diffusion is a larger problem in the 4° × 5° resolution run than in the 2° × 2.5° run (compare Figs. 6a and 6b). Main features, although placed as accurately as before, are more diffuse. The 120°–300°E total ozone gradient is nearly indistinguishable. Current experiments are being run at the 2° × 2.5° resolution.

The spectral calculation is less successful, especially near the pole. The distinguishing features are still present, but the most noticeable feature is the ringing structure that seems to emanate from the excessively large 270°E high. The transport winds are very noisy near the poles. The spectral fit to these winds near the poles is inaccurate and transport by these winds is responsible for this ringing structure. This structure seriously contaminates the polar vortex.

An attribute of van Leer's method is that it is able to maintain gradients better than spectral calculations. However, the meridional ozone gradients at low latitudes in both the spectral and van Leer calculations are larger than observed. The gradients are exaggerated by the projection, but the main cause is excessively large vertical transport, which is a consequence of the

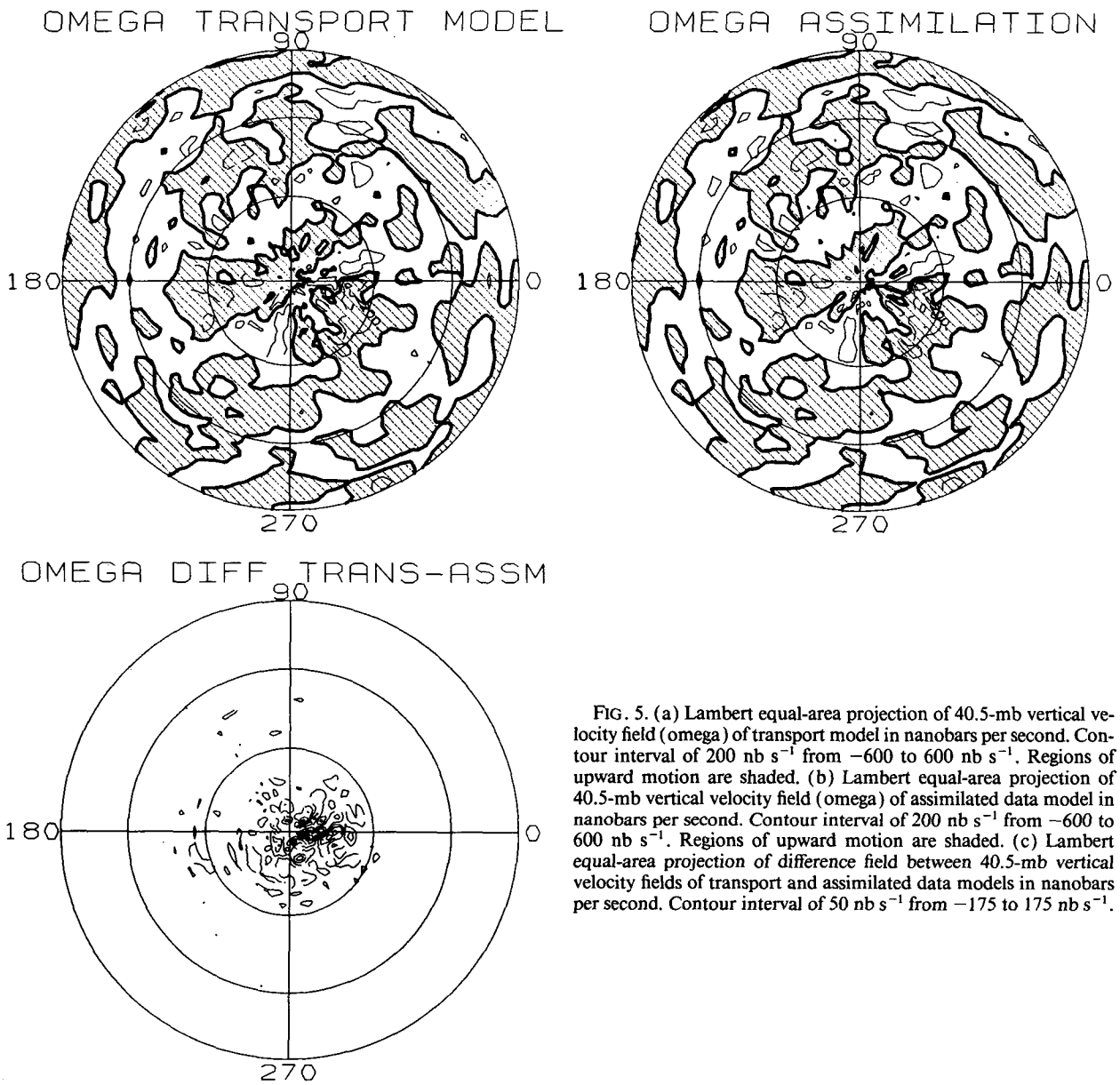

FIG. 5. (a) Lambert equal-area projection of 40.5-mb vertical velocity field (omega) of transport model in nanobars per second. Contour interval of 200 nb s^{-1} from -600 to 600 nb s^{-1}. Regions of upward motion are shaded. (b) Lambert equal-area projection of 40.5-mb vertical velocity field (omega) of assimilated data model in nanobars per second. Contour interval of 200 nb s^{-1} from -600 to 600 nb s^{-1}. Regions of upward motion are shaded. (c) Lambert equal-area projection of difference field between 40.5-mb vertical velocity fields of transport and assimilated data models in nanobars per second. Contour interval of 50 nb s^{-1} from -175 to 175 nb s^{-1}.

meridional circulation being too strong in the assimilated data (see Rood et al. 1991).

Spectral transport can be accurate, and spectral schemes can be made monotonic. However, because the spectral method provides global fits to what may be localized source and sink terms, they can be problematic in atmospheric applications. Experience with low- and medium-resolution spectral methods shows that the numerical difficulties associated with fitting spherical harmonics to real atmospheric wind fields that contain noise severely impact the transport calculation. This would not necessarily be a problem for model winds from a spectral calculation. However, spectral transport has proven to be problematic in atmospheric applications (Williamson and Rasch 1989).

4. Summary

The scheme of van Leer (1974; 1977a,b; 1979) has been used to demonstrate the application of upstream-biased monotonic schemes to atmospheric problems. The major disadvantage of the scheme is a self-limiting diffusion that manifests itself with a shape-preferring characteristic. Similar schemes in the class have less diffusion (e.g., Zalesak 1987). The van Leer scheme was chosen because of its simplicity and its known

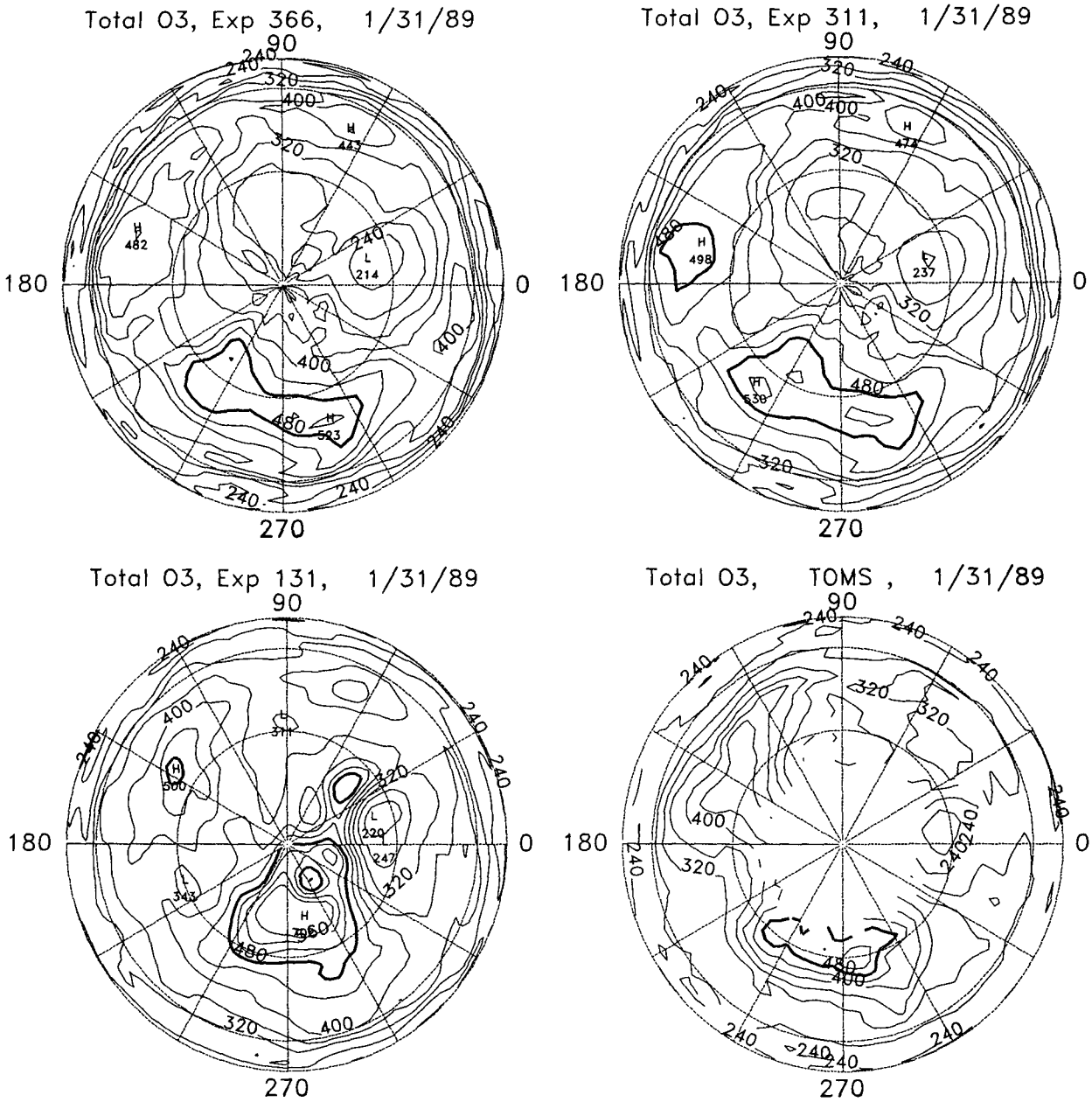

FIG. 6. Polar orthographic projection of total ozone field in Dobson units on 31 January 1989 from (a) van Leer calculation with a 2° × 2.5° resolution, (b) van Leer calculation with a 4° × 5° resolution, (c) an R30 spectral calculation, and (d) TOMS measurements.

ability to be time split. Many schemes do not maintain their accuracy when time split or when applied to curvilinear coordinates.

Constituent correlations have proven to be a valuable tool to interpret chemical and dynamical processes. An advantage of the scheme is its ability to maintain constituent correlations. Constituent correlations are degraded whenever the partitioning of constituents between boxes by the transport algorithm is constituent dependent. An example of constituent-dependent partitioning is filling. Nonmonotonic transport schemes such as spectral transport may require filling to maintain positive mixing ratios. An upstream-biased transport algorithm determines the partitioning as a function of velocity. A monotonic upstream-biased algorithm such as van Leer's method will maintain constituent correlations as long as the monotonicity algorithm does not mix mass between adjoining boxes.

The van Leer scheme has been successfully applied to seasonal integrations of stratospheric chemistry (Rood et al. 1991). With 2° latitude × 2.5° longitude resolution, we can maintain the vortex edge and simulate many of the features of the Airborne Arctic Stratosphere Expedition data.

Acknowledgments. We thank Eric Nash for his help in solving the continuity equation and Pam Redmond for her assistance in preparing this manuscript. We would like to thank an anonymous referee for many useful comments that improved the manuscript. Contribution 62 of the Stratospheric General Circulation with Chemistry Project at NASA/GSFC.

REFERENCES

Baker, W. E., S. C. Bloom, J. S. Woollen, M. S. Nestler, E. Brin, T. W. Schlatter and G. W. Branstator, 1987: Experiments with a three-dimensional statistical objective analysis scheme using FGGE data. *Mon. Wea. Rev.*, **115,** 272–296.

Douglass, A. R., R. B. Rood, R. S. Stolarski, M. R. Schoeberl, M. H. Proffitt, J. J. Margitan, M. Loewenstein, J. R. Podolske and S. E. Strahan, 1990: Global three-dimensional constituent fields derived from profile data. *Geophys. Res. Lett.*, **17,** 525–528.

Fahey, D. W., K. K. Kelly, S. R. Kawa, A. F. Tuck, M. Loewenstein, K. R. Chan and L. E. Heidt, 1990a: Observations of denitrification and dehydration in the winter polar stratospheres. *Nature,* **344,** 321–324.

——, S. Solomon, S. R. Kawa, M. Loewenstein, J. R. Podolske, S. E. Strahan and K. R. Chan, 1990b: A diagnostic for denitrification in the winter polar stratospheres. *Nature,* **345,** 698–702.

Forester, C. K., 1977: High order monotonic convective difference schemes. *J. Comput. Phys.*, **23,** 1–22.

Haltiner, G. J., and R. T. Williams, 1980: *Numerical Prediction and Dynamic Meteorology.* John Wiley and Sons, 477 pp.

Hawley, J. F., L. L. Smarr and J. R. Wilson, 1984: A numerical study of nonspherical black hole accretion. II: Finite differencing and code calibration. *Ap. J. Suppl.*, **55,** 211–246.

Kaye, J. A., R. B. Rood and D. J. Allen, 1989a: Variability of chlorine containing species as revealed by three-dimensional stratospheric and chemistry models. *Ozone in the Atmosphere. Proc. of the Quadrennial Ozone Symp. 1988 and Tropospheric Ozone Workshop,* Gottingen, Federal Republic of Germany, Rumen D. Bojkov and Peter Fabian, Eds., A. Deepak Publishing, 676–679.

——, R. B. Rood, D. J. Allen, E. M. Larson and C. H. Jackman, 1989b: Three-dimensional simulation of spatial and temporal variability of stratospheric hydrogen chloride. *Geophys. Res. Lett.*, **16,** 1149–1152.

——, A. R. Douglass, R. B. Rood, R. S. Stolarski, P. A. Newman, D. J. Allen, E. M. Larson, M. T. Coffey, W. G. Mankin and G. C. Toon, 1990: Three-dimensional simulation of HCl and HF during the AASE. *Geophys. Res. Lett.*, **17,** 529–532.

McRae, G. J., W. R. Goodin and J. H. Seinfeld, 1982: Numerical solution of the atmospheric diffusion equation for chemically reacting flows. *J. Comput. Phys.*, **45,** 1–42.

Newman, P. A., L. R. Lait and M. R. Schoeberl, 1988: The morphology and meteorology of Southern Hemisphere spring total ozone miniholes. *Geophys. Res. Lett.*, **15,** 923–926.

Rood, R., 1987: Numerical advection algorithms and their role in atmospheric transport and chemistry models. *Rev. Geophys.*, **25,** 71–100.

——, D. J. Allen, W. E. Baker, D. J. Lamich and J. A. Kaye, 1989a: The use of assimilated stratospheric data in constituent transport calculations. *J. Atmos. Sci.*, **46,** 687–701.

——, J. A. Kaye, D. J. Allen, W. E. Baker and D. J. Lamich, 1989b: The use of winds and temperatures from a stratospheric assimilation model in three-dimensional constituent transport studies. *Ozone in the Atmosphere. Proc. of the Quadrennial Ozone Symp. 1988 and Tropospheric Ozone Workshop,* Gottingen, Federal Republic of Germany, Rumen D. Bojkov and Peter Fabian, Eds., A. Deepak Publishing, 625–629.

——, ——, A. R. Douglass, D. J. Allen, S. D. Steenrod and E. M. Larson, 1990: Wintertime nitric acid chemistry: Implications from three-dimensional model calculations. *J. Atmos. Sci.*, **47,** 2696–2709.

——, A. R. Douglass, J. A. Kaye, M. A. Geller, C. Yue-Chen, D. J. Allen, E. M. Larson, E. R. Nash and J. E. Nielsen, 1991: Three-dimensional simulations of wintertime ozone variability in the lower stratosphere. *Geophys. Res. Lett.*, **96,** 5055–5071.

Thompson, J. F., 1984: Convection schemes for use with curvilinear coordinate systems—a survey. Misc. Pap. E-84-4, 262 pp. [Available from U.S. Army Corps of Eng., Dept. of the Army, Washington, D.C. 20314.]

van Leer, B., 1974: Towards the ultimate conservative difference scheme. II: Monotonicity and conservation combined in a second-order scheme. *J. Comput. Phys.*, **14,** 361–370.

——, 1977a: Towards the ultimate conservative difference scheme. III: Upstream-centered finite-difference schemes for ideal incompressible flow. *J. Comput. Phys.*, **23,** 263–275.

——, 1977b: Towards the ultimate conservative difference scheme. IV: A new approach to numerical convection. *J. Comput. Phys.*, **23,** 276–299.

——, 1979: Towards the ultimate conservative difference scheme. V: A second order sequel to Godanov's Method. *J. Comput. Phys.*, **32,** 101–136.

Williamson, D. L., and P. J. Rasch, 1989: Two-dimensional semi-Lagrangian transport with shape-preserving interpolation. *Mon. Wea. Rev.*, **117,** 102–129.

Zalesak, S. T., 1987: A preliminary comparison of modern shock-capturing schemes: Linear advection. *Advances in computer methods for partial differential equations VI,* R. Vichnevetsky and R. S. Stepleman, Eds., IMACS publ., 15–22.